Velocity saturation in intrinsic graphene

2009 J. Phys.: Condens. Matter 21 344201

(http://iopscience.iop.org/0953-8984/21/34/344201)

IOP Publishing Journal of Physics: Condensed Matter

J. Phys.: Condens. Matter **21** (2009) 344201 (5pp) doi:10.1088/0953-8984/21/34/344201

Velocity saturation in intrinsic graphene

R S Shishir and D K Ferry

Department of Electrical Engineering and Center for Solid State Electronics Research, Arizona State University, Tempe, AZ 85287, USA

E-mail: shishir@asu.edu

Received 27 April 2009, in final form 22 May 2009
Published 27 July 2009
Online at stacks.iop.org/JPhysCM/21/344201

Abstract

We study the transport of carriers in intrinsic graphene by means of an ensemble Monte Carlo technique. Scattering by acoustic and optical phonons dominates the transport. We find that velocity 'saturation' sets in at relatively low values of the electric field, but that the value is dependent upon the carrier density. Velocity overshoot is also observed to occur in these simulations.

(Some figures in this article are in colour only in the electronic version)

The behavior of energetic electrons in semiconductors has been of interest since the first studies into the breakdown and current saturation of these materials [1, 2]. Only strong metals seem to maintain linear behavior to high electric fields [3]. But, graphene is a strange metallic material, with somewhat conflicting device characteristics. Graphene is one of the remarkable discoveries made in the last century, with serious interest arising in 2004 when A Geim and his group were successfully able to extract graphene in its two-dimensional form by mechanical exfoliation [4]. After that, a great deal of theoretical and experimental interest has been generated to investigate its rather unusual behavior and for possible applications in future technology [5]. The interest seems to originate from the astonishing difference between graphene and other well known two-dimensional semiconductor systems. In graphene, the atoms are arranged into a honeycomb lattice and produce a unique bandstructure, where the bands and electron transport are mainly influenced by the linear energy bands near the Dirac point [6].

Although intense theoretical studies have focused upon graphene's transport [7–11], there apparently have been no reports of high electric field behavior in graphene to date. The possibility of graphene's application in future nanoscale devices greatly depends on its transport properties at high electric field, and a comprehensive understanding of high field transport is a must. Meric *et al* have observed current saturation in graphene field-effect transistors as expected by electrostatic depletion from the gate [12], whereas Lin *et al*, observe little effect of the gate in similar transistors [13], the latter behavior expected from the Klein paradox where electrons tunnel through finite length barriers without reflection [14]. While Meric *et al* considered the possibility of velocity saturation, in fact little is presently known about this phenomenon in graphene. On the other hand, it is known from ensemble Monte Carlo studies, that velocity saturation does occur in carbon nanotubes, the rolled up version of graphene [15]. In this paper, we conduct a systematic study of velocity saturation in graphene as a function of electron density and electric field. Here, we use an ensemble Monte Carlo procedure to solve the Boltzmann transport equation with the unique graphene band structure. We find that the value of the saturation velocity is a function of the electron density itself, with strong saturation, and even negative differential conductance, being observed.

In this approach, an ensemble of particles is subjected alternatively to acceleration in an applied electric field, and scattering by the various phonons that are active in the material [16]. An essential part of the process is treatment of the density of states in the linear band and degeneracy that occurs in graphene at reasonable densities. This degeneracy is incorporated by a rejection process which accounts for occupancy of the final state after scattering [17]. Then various parameters such as average energy, distribution function, and velocity are computed by taking an ensemble average over the carriers involved in the transport. An ensemble of 10^5 particles is used in this study. Usually, the value of mass is required to determine drift velocity in any material. But graphene is an extraordinary material whose band structure is governed by the Dirac equation, in which charge carriers imitate relativistic particles with zero *rest* mass. Away from the Dirac point, its mass is found easily by relating the crystal momentum to the particle momentum, which yields a result that is the same as the cyclotron mass, and which therefore varies linearly with the energy or momentum [18]. We then calculate the drift velocity

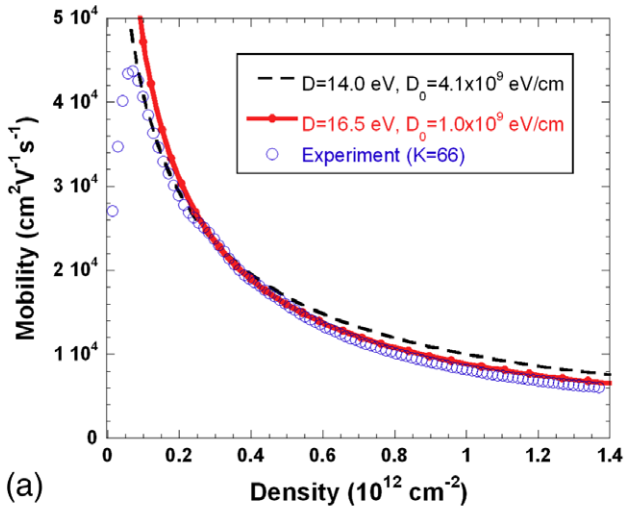

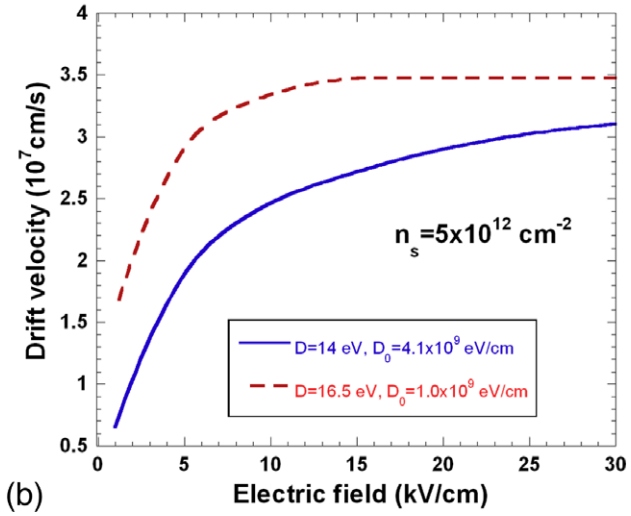

Figure 1. (a) The experimental mobility for the case of $K = 66$, taken from [20]. We plot two mobility curves for comparison, where these are determined for two sets of coupling constants. These are discussed in the text. (b) The velocity plotted as a function of the electric field for these two sets of parameters used in panel (a), and a density of 5×10^{12} cm^{-2}.

in graphene from the relationship

$$v_{\rm d} = \left\langle \frac{\hbar k_y}{m^*} \right\rangle = \left\langle \frac{\hbar k_y}{\hbar k / v_{\rm F}} \right\rangle = v_{\rm F} \left\langle \frac{k_y}{k} \right\rangle, \tag{1}$$

where the angular brackets denote the ensemble average

$$\langle A \rangle = \frac{1}{N} \sum_i A_i, \tag{2}$$

and A is any parameter of interest. In (1), $v_{\rm F}$ is the Fermi velocity of the carriers in the linear Dirac band, k is the value of the total momentum and k_y is the wavevector along the electric field.

Here, we are interested in the intrinsic, phonon limited velocity behavior in graphene at room temperature. Most studies of the transport at room temperature have involved limited mobility due to the impact of impurities in the SiO_2 upon which the exfoliated graphene is deposited.

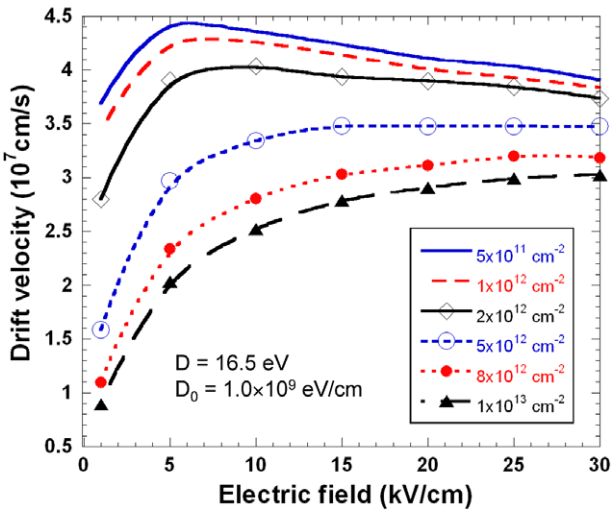

Figure 2. The steady state drift velocity is plotted as a function of applied field for different carrier densities.

Recently, however, these layers have been immersed in various polar liquids with relatively high dielectric constants, which screened the impurity Coulomb interaction and resulted in high mobilities at room temperature [19]. In this case, the liquid apparently penetrates between the graphene and the oxide to enhance the screening of the impurities in the oxide. Mobilities above 40 000 cm^2 V^{-1} s^{-1} were found. This has uncovered what we believe to be the intrinsic mobility at various densities and allowed us to determine the coupling constant for the acoustic phonons and to estimate the coupling constant for the optical phonons [20]. In studying the 'intrinsic' mobility in graphene, Chen *et al* [21] considered acoustic modes of the graphene phonons, but neglected the optical modes. Instead, they assumed that remote interface modes [22], derived from the polar interaction in SiO_2, would be important. But, these modes are known to not be very important, even in the Si/SiO_2 case [23, 24]. Moreover, the interaction of these modes is predominantly Coulombic in nature, and this will be screened by the high dielectric constant materials. Instead, we consider scattering by the non-polar optical phonons, arising from the K point phonons, which couple the K and K' valleys of the conduction band. From studies of the phonon structure, this is the LA + LO mode with an energy of 150 meV [25]. Both the long wavelength intra-valley optical mode and the zone edge TA mode are forbidden by symmetry [26], and there is an out-of-plane mode near the latter that can give rise to ripple modes in second order [27]. In the rigid ion approximation, and with a deformation field D_0 and optical phonon frequency ω_0, the scattering rate becomes

$$\frac{1}{\tau} = \frac{D_0^2}{\rho_{\rm m}\omega_0(\hbar v_{\rm F})^2}[(E - \hbar\omega_0)(N_q + 1)u_0(E - \hbar\omega_0) + (E + \hbar\omega_0)N_q]. \tag{3}$$

Here, $\rho_{\rm m}$ is the areal mass density of graphene, N_q is the Bose–Einstein distribution for the phonons, and u_0 is the Heaviside function ($u_0 = 1$ for the argument $\geqslant 0$ and zero otherwise). The other symbols have their normal meaning. The function u_0 assures that the energy is sufficient to emit a phonon. For

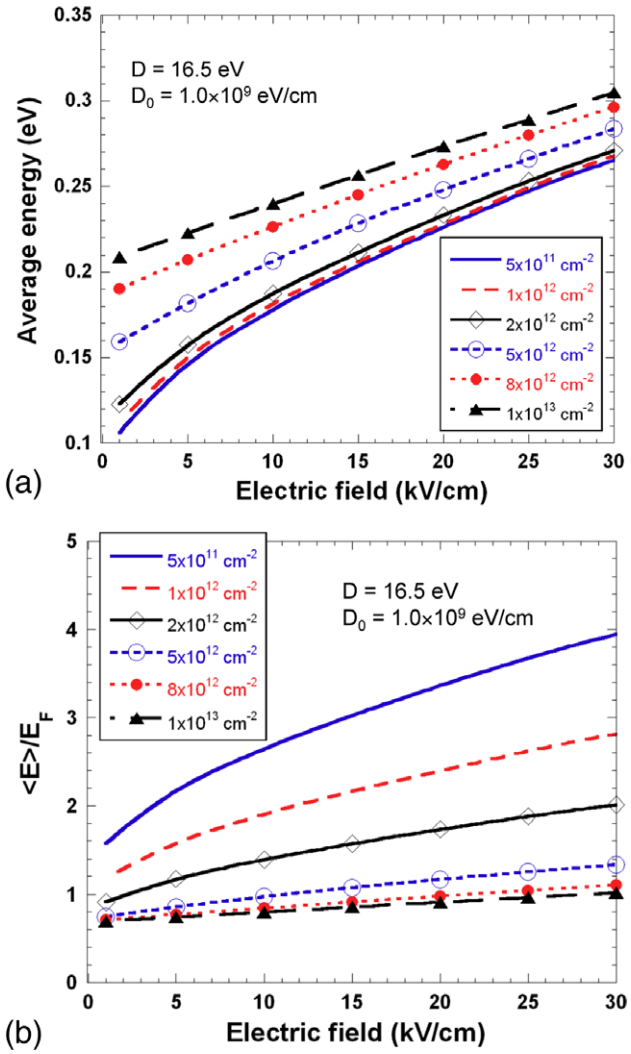

Figure 3. (a) The average energy attained by the carriers as a function of electric field. (b) This same energy normalized to the equilibrium Fermi energy at that density.

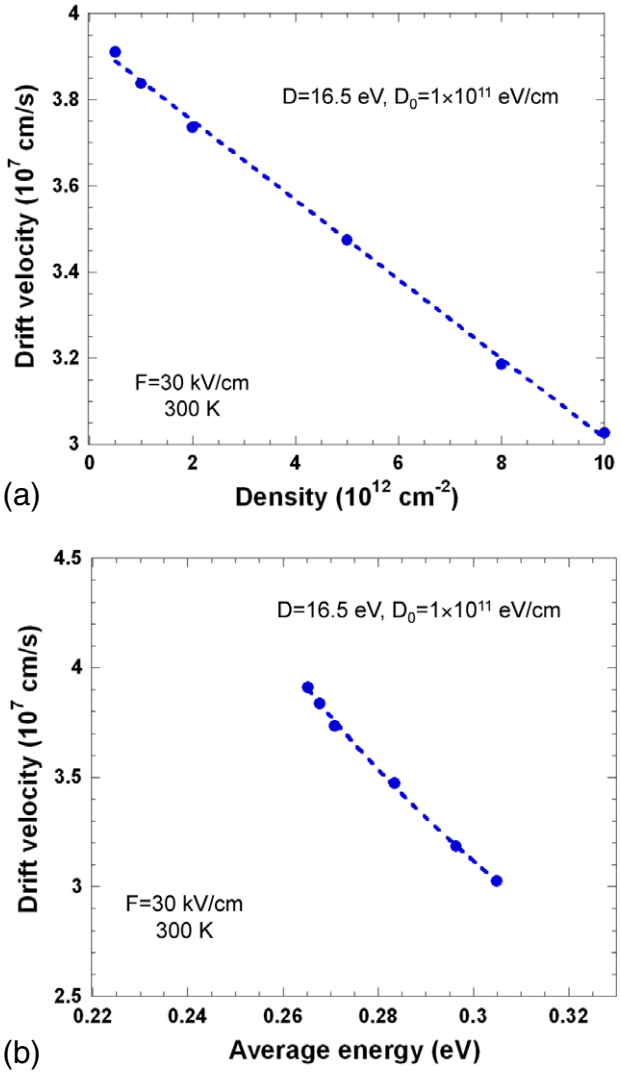

Figure 4. The steady state velocity at 30 kV cm^{-1} as a function of the (a) carrier density and (b) the average energy attained at this field.

acoustic phonons, the scattering rate derived by Hwang and Das Sarma [28] for the equipartition limit (high temperature, and corrected for an apparent typographical error) is given as

$$\frac{1}{\tau(E)} = \frac{4D^2 k_B T}{\hbar^3 \rho_m (v_{ph} v_F)^2} E(k). \tag{4}$$

Here, D is the acoustic deformation potential, v_{ph} is the sound velocity, and k_B is Boltzmann's constant. We include only these scattering mechanisms in the calculation. In figure 1(a), we plot the experimental mobility for the case of $K = 66$ (K is the relative dielectric constant), taken from [20]. We plot two mobility curves for comparison, where these are determined for two sets of coupling constants. In one case, we use $D = 14$ eV for the acoustic modes and $D_0 = 4.1 \times 10^9$ eV cm^{-1} for the optical mode. In the other, the coupling constants used are $D = 16.5$ eV for the acoustic modes and $D_0 = 10^9$ eV cm^{-1} for the optical mode. The former case gives a slightly better fit at very low density, but is not a particularly good fit at high density. This would require an additional scattering process to be incorporated. The latter case, gives a very good fit at higher density, but not so good at low density. However, Coulomb scattering will improve this low density fit. As mentioned above, these values lead to a room temperature mobility above 40 000 cm^2 V^{-1} s^{-1} at room temperature in what is believed to be intrinsic graphene. In figure 1(b), we plot the velocity as a function of the electric field for these two cases, and a density of 5×10^{12} cm^{-2}. We see that only the latter set of coupling constants give a good saturation, while the velocity is higher for this set. This occurs as the stronger optical coupling leads to a higher energy loss, with the resulting lower average energy (and consequently a lower value of effective mass). Our preference is to use this latter set of parameters, and we do not consider the first set further.

In figure 2, we plot the steady state drift velocity as a function of applied field for different carrier densities. Remarkably, we find that the onset of saturated behavior occurs at lower field, and the value of velocity is higher, with lower carrier density. In fact, at low density, we even observe

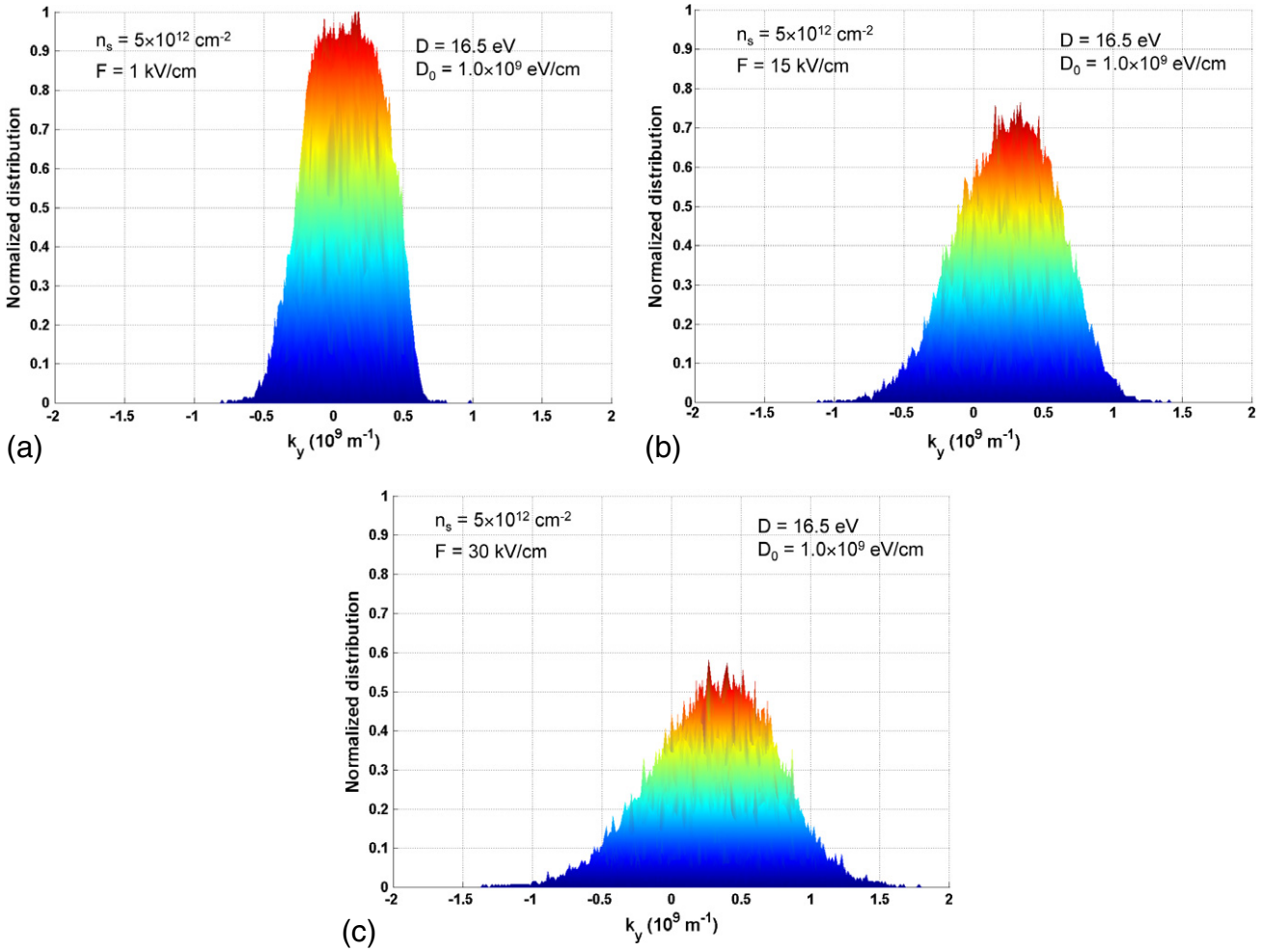

Figure 5. The particle distribution along the field direction for three different values of the electric field: (a) 1 kV cm^{-1}, (b) 15 kV cm^{-1}, (c) 30 kV cm^{-1}. This is done for a carrier density of 5×10^{12} cm^{-2}.

a negative differential conductance, in which the velocity actually decreases with increasing electric field. Graphene has a linear dispersion relationship around the Dirac point. So, its energy increases linearly with increasing total momentum. But the mass also increases linearly with the energy. Therefore, at lower carrier density, the phonon scattering decreases, and the mass also decreases, both of which lead to a higher velocity. In the low density region, the average mass increases as the energy is increasing, and this leads to the observation of negative differential conductance. As we raise the density, the scattering, average energy, and mass all increase, leading to lower velocities for the carriers.

In figure 3(a), we plot the average energy attained by the carriers as a function of electric field. This is plotted for the same densities as shown in figure 2. In figure 3(b), we plot the same data, but now the average energy is normalized to the Fermi energy in the electron gas. Here, we note that the average energy at low fields is given by $2E_F/3$, for the higher carrier densities. In fact, this is the value expected for a degenerate electron gas in graphene in equilibrium. At lower densities, this value rises as the distribution is considerably less degenerate at these low densities. At high fields, we note that the curves tend to converge toward each other in figure 3(a).

In figures 4(a) and (b), we plot the steady state velocity at 30 kV cm^{-1} as a function of the carrier density and the average energy attained at this field. It may be seen that the latter satisfies a power law (near quadratic) fit, which reveals an inverse square relationship present between the velocity and average energy. In fact, this is what expected from graphene. To elaborate, we consider that at any value of the field, there is an effective (chordal) mobility relating the velocity to this field, as

$$v = \mu F = \frac{e\tau}{m^*} F. \tag{5}$$

For graphene, as mentioned before, the effective mass increases linearly with energy, while the relaxation time has an inverse relation with energy through its connection to the density of states. As a result, to first order, it may be expected that the velocity will decrease with the square of the energy, and this is very nearly the situation described by figure 4. In figure 4(a), where we plot the velocity at 30 kV cm^{-1} as a function of the density, we can see that drift velocity decreases linearly with increasing density, consistent with the arguments above.

In figure 5, we illustrate how the initial Fermi–Dirac distribution is broadened and shifted in the high electric field.

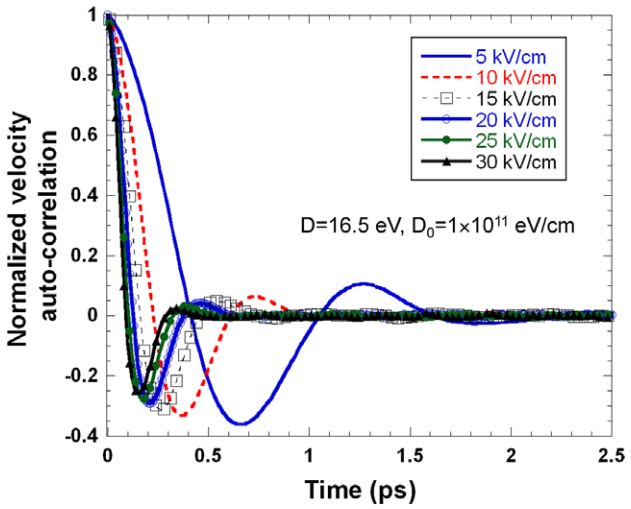

Figure 6. The velocity autocorrelation function for various values of the electric field and for a carrier density of 5×10^{12} cm^{-2}.

In figure 5, we plot the projection of the particle distribution along the electric field direction as a function of momentum for three different values of the electric field and for a carrier density of 5×10^{12} cm^{-2}. From these plots, it is clear to see that there is a change in both the average energy (change in the Fermi energy) and in the temperature (broadening of the distribution) as the field is increased.

Finally, in figure 6, we plot the velocity autocorrelation function for the ensemble, starting from the initial time $t = 0$, for several values of the electric fields and a carrier density of 5×10^{12} cm^{-2}. Here, this function is defined as

$$\frac{1}{N\langle v^2(0)\rangle}\sum_{i=1}^{N} v_i(0)v_i(t). \tag{6}$$

The non-monotonic behavior of the autocorrelation function is a clear sign of velocity overshoot [29], which occurs at almost all densities and sets in at very low values of the electric field. At higher fields, the curves begin to overlap, showing that the relaxation times and duration of overshoot phenomena are saturating at a common set of times.

In summary, anomalous velocity saturation that is velocity saturation behavior different than observed in normal semiconductors, is observed in intrinsic graphene at room temperature when only phonon scatterings are considered. The reason behind this anomaly lies in graphene's unique bandstructure which has a linear dispersion relation near the Dirac point. The saturated velocities show a systematic variation with both the average energy and the carrier density. Here, we have only extended the electric field up to 30 kV cm^{-1}, but one could go further. However, we have considered only the simple Dirac band structure, and it is known that distortions of the energy surface occur at higher energies than we have gone here. To probe to higher electric fields and higher carrier energies, it is likely that one will have to incorporate the full band structure to account for these deviations from the simple Dirac band form.

Acknowledgments

The authors have benefited from helpful discussions with S M Goodnick, M Saraniti, J P Bird, J Kono, Y Ochiai, and R Akis.

References

[1] Fröhlich H and Seitz F 1950 *Phys. Rev.* **79** 526
[2] Ryder E J 1953 *Phys. Rev.* **90** 766
[3] Heinrich H and Jantsch W 1969 *Solid State Commun.* **7** 377
[4] Novoselov K S *et al* 2004 *Science* **306** 666
[5] Castro Neto A H *et al* 2009 *Rev. Mod. Phys.* **81** 109
[6] Wallace P R 1947 The band theory of graphite *Phys. Rev.* **71** 622
[7] Hwang E H, Adam S and Das Sarma S 2007 *Phys. Rev. Lett.* **98** 186806
[8] Adam S *et al* 2007 *Proc. Natl Acad. Sci. USA* **104** 18392
[9] Ando T 2006 *J. Phys. Soc. Japan* **75** 074716
[10] Aleiner I and Efetov K 2006 *Phys. Rev. Lett.* **97** 236801
[11] Nomura K and MacDonald A H 2007 *Phys. Rev. Lett.* **98** 076602
[12] Meric I *et al* 2009 *Nat. Nanotechnol.* **3** 654
[13] Lin Y-M *et al* 2009 *Nano Lett.* **9** 422
[14] Katsnelson M *et al* 2006 *Nat. Phys.* **2** 620
[15] Verma A, Kauser M Z and Ruden P P 2005 *J. Appl. Phys.* **97** 114319
[16] Jacoboni C and Lugli P 1990 *The Monte Carlo Method for Semiconductor Device Simulation* (Heidelberg: Springer)
[17] Lugli L and Ferry D K 1985 *IEEE Trans. Electron Devices* **32** 2431
[18] Novoselov K S *et al* 2005 *Nature* **438** 197
[19] Chen F *et al* 2009 *Nano Lett.* **9** 2571–4
[20] Shishir R and Ferry D K 2009 *J. Phys.: Condens. Matter* **21** 232204
[21] Chen J H, Jang C, Xiao S, Ishigami M and Fuhrer M S 2008 *Nat. Nanotechnol.* **3** 206
[22] Hess K and Vogl P 1979 *Solid State Commun.* **30** 807
[23] Moore B T and Ferry D K 1980 *J. Vac. Sci. Technol.* **17** 1037
[24] Moore B T and Ferry D K 1980 *J. Appl. Phys.* **51** 2603
[25] Yanagisawa H, Tanaka T, Ishida Y, Matsue M, Rokuta E, Otani S and Oshima C 2005 *Surf. Interface Anal.* **37** 133
[26] Mañes J L 2007 *Phys. Rev.* B **76** 045430
[27] Morozov S V, Novoselov K S, Katsnelson M I, Schedin F, Elias D C, Jaszczak J A and Geim A K 2008 *Phys. Rev. Lett.* **100** 016602
[28] Hwang E H and Das Sarma S 2008 *Phys. Rev.* B **77** 115449
[29] Ferry D K and Barker J R 1981 *J. Appl. Phys.* **52** 818